ELSEVIER

Journal of Magnetism and Magnetic Materials 189 (1998) 263–273

Journal of magnetism and magnetic materials

Magnetic properties of random-anisotropy amorphous magnets $(R_xFe_{1-x})_{80}Si_{12}B_8$ with R = Pr, Nd, Sm, Tb, Dy and Er

H. Kato[a,*], N. Kurita[a,1], Y. Ando[a], T. Miyazaki[a], M. Motokawa[b]

[a] *Department of Applied Physics, Graduate School of Engineering, Tohoku University, Sendai 980-8579, Japan*
[b] *Institute for Materials Research, Tohoku University, Sendai 980-8577, Japan*

Received 12 March 1998; received in revised form 8 July 1998

Abstract

Magnetic properties of rapidly quenched amorphous alloys $(R_xFe_{1-x})_{80}Si_{12}B_8$ with R = Pr, Nd, Sm, Tb, Dy and Er ($0.1 \leqslant x \leqslant 1.0$) have been investigated systematically by Mössbauer absorption and magnetization measurements in fields of up to 300 kOe. Mössbauer experiments have shown that the averaged Fe magnetic moment decreases rapidly with increasing x. Low-field magnetic measurements have exhibited a spin-freezing behavior at low temperatures in all R-rich samples. The freezing temperature T_f rapidly decreases with increasing magnitude of magnetic field H. High-field magnetization isotherms at low temperatures showed a large hysteresis, in which the coercive field H_c increases rapidly with decreasing temperature. In H–T space, the lines of $H_c(T)$ and $T_f(H)$ are found to be almost identical, which have therefore been regarded as a boundary between reversible and irreversible regions in the magnetic phase diagram. Upward concavity in the high-field magnetization curve has been observed in R = Tb and Dy samples with $x = 0.2$, which was suggested to be an incipient stage of a transition from sperimagnetic to asperomagnetic state, based on the numerical calculations.

PACS: 75.30.K; 75.50.K; 75.50.L

Keywords: Anisotropy – random; High-field magnetization; Correlated spin glass

1. Introduction

For more than two decades much effort has been spent on the experimental and theoretical studies of random magnets, in which the orientation of magnetic moment distributes randomly and freezes at low temperatures. A typical example is a diluted magnetic alloy such as Au–Fe system. The origin of spin freezing behavior observed in this system has been attributed to the RKKY-like fluctuation of exchange interaction between the Fe atoms distributed randomly. On the other hand, it is well known that the amorphous alloys containing rare-earth

* Corresponding author. Tel.: + 81 22 217 7948; fax: + 81 22 217 7947; e-mail: kato@mlab.apph.tohoku.ac.jp.

[1] Present address: Central Res. Lab., Hitachi Ltd., Kokubunji 185-8601, Japan.

0304-8853/98/$19.00
PII: S0304-8853(98)00285-6

(R) and Fe also show a spin freezing behavior at low temperatures [1,2]. In this case, the origin of the freezing is considered to be the large random magnetic anisotropy (RMA), which originates from a random distribution of principal directions of crystalline electric field (CEF) potentials at R sites. As a result of RMA, the magnetic structure is not a simple ferromagnetic or ferrimagnetic, but will be a sperimagnetic or speromagnetic one [1,2], depending on the relative magnitude of RMA with respect to the exchange energy. Chudnovsky and coworkers [3,4] proposed a correlated spin glass (CSG) state for small RMA system. They also stated that, under a large external field or strong coherent anisotropy, CSG state will be modified so as to behave like a ferromagnet, which is called a ferromagnet with wandering axes (FWA) state.

On the other hand, binary R–Fe amorphous alloys have been studied extensively not only for their physical interest but also for technological importance for permanent magnets, magnetostrictive materials, and magneto-optical recording materials. It is therefore important to investigate systematically the magnetic properties of R–Fe alloys as a function of R concentration. However, it is not easy to obtain amorphous alloys of binary R–Fe system over the wide concentration range, which is mainly due to the structural instability of the amorphous phase. To investigate the relation between RMA and R content systematically, we have prepared the pseudo-binary amorphous alloys of $(R_xFe_{1-x})_{80}Si_{12}B_8$ with R = Pr, Nd, Sm, Tb, Dy and Er over the entire range of x by using a rapidly quenching method. In this paper, we report detailed studies of low-field and high-field magnetization measurements together with Mössbauer absorption experiments in these pseudo-binary amorphous alloys.

2. Experimental

Alloys of $(R_xFe_{1-x})_{80}Si_{12}B_8$ with R = Pr, Nd, Sm, Tb, Dy, Er; and $0.1 \leqslant x \leqslant 1$ were prepared by arc melting under atmospheric Ar gas. The purity of the starting materials used was at least 99.9%. By using these buttons of polycrystalline materials, we obtained amorphous ribbons of about 1 mm in width, 20 cm in length and 20 μm in thickness by a single-roller rapidly quenching method in an Ar atmosphere with the surface velocity of 50–70 m/s. The amorphous structure was confirmed by X-ray diffraction using Cu K_α radiation.

Measurements of magnetization of up to 55 kOe were performed by using a SQUID magnetometer of Quantum Design Inc. The zero-field-cooled (ZFC) magnetization was measured on heating after cooling to the lowest temperature at zero field, while the field-cooled (FC) magnetization was measured on cooling after the field was applied at the highest temperature. High-field magnetization measurements of up to 150 kOe generated by a high-power water-cooled magnet were performed by using VSM system. A sample-extraction magnetometer was used for measurements in fields of up to 300 kOe generated by a hybrid magnet [5]. Mössbauer absorption measurements at zero field were carried out at 10 K by using a constant-acceleration method with a source of ^{57}Co.

3. Results and discussions

3.1. Mössbauer absorption

First, we show the results of Mössbauer experiments, which have been performed to trace the change in Fe magnetic moments as a function of the R concentration x. Fig. 1a shows the example of observed spectra for samples with R = Tb obtained at 10 K. Observed spectra exhibit a considerable broadening of absorption peaks, suggesting a significant distribution of hyperfine fields H_{hf} at the Fe nuclei. Although broadened, six definite peaks can be identified for the $x = 0.1$ sample, which become obscure and merged into single broad peak in the $x = 0.8$ sample. Probability of hyperfine-field distribution $P(H_{hf})$ is plotted as a function of H_{hf} in Fig. 1b, by using both Hesse [6] and Window [7] methods. The results for the two methods are in good agreements, and calculated spectra by the latter method, given by the solid lines in Fig. 1a, well reproduce the observation. Averaged hyperfine field $\langle H_{hf} \rangle$, indicated by arrows in Fig. 1b, decreases with increasing x; for the $x = 0.8$ sample being less than 100 kOe. It should be noted that the

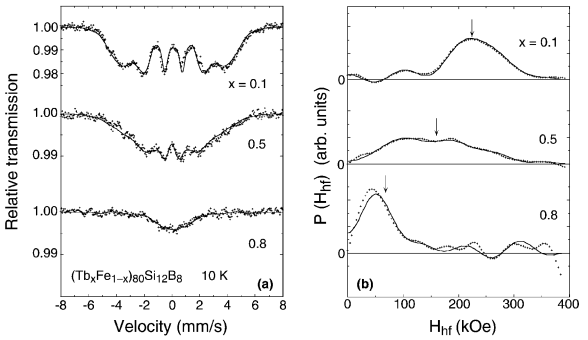

Fig. 1. (a) ^{57}Fe Mössbauer spectra for $(Tb_xFe_{1-x})_{80}Si_{12}B_8$ amorphous alloys with $x = 0.1$, 0.5 and 0.8 observed at 10 K. Solid curves represent the best-fit calculations by using the Window [7] method. (b) Probability of hyperfine-field distribution $P(H_{hf})$ obtained by using Hesse (solid lines) [6] and Window (dotted lines) methods. Arrows in (b) denote the averaged hyperfine field $\langle H_{hf} \rangle$.

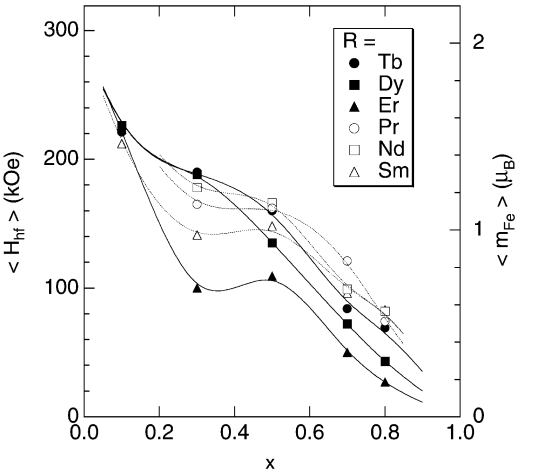

Fig. 2. Concentration dependence of averaged hyperfine fields $\langle H_{hf} \rangle$ in $(R_xFe_{1-x})_{80}Si_{12}B_8$. Averaged Fe magnetic moment values $\langle m_{Fe} \rangle$ are also shown in the right ordinate.

distribution of the hyperfine fields becomes much significant in the sample with $x = 0.5$. Similar spectra have been obtained for samples with R = Dy and Er, and for light R samples with R = Pr, Nd and Sm. Concentration dependence of averaged hyperfine fields $\langle H_{hf} \rangle$ in the heavy R and light R samples are shown in Fig. 2. The values of $\langle H_{hf} \rangle$ decrease rapidly with increasing x, although there are distinct plateaus between $0.3 \leqslant x \leqslant 0.5$ except for R = Tb and Dy. If we convert the $\langle H_{hf} \rangle$ values to the Fe magnetic moment by using the ratio 145 kOe/μ_B [8], as indicated by the right ordinate in Fig. 2, then $\langle m_{Fe} \rangle$ is reduced to about 1 μ_B for $x = 0.5$. Similar reduction of Fe magnetic moment with increasing x was reported for $(Gd_xFe_{1-x})_{80}Si_{12}B_8$ [9].

3.2. Magnetic phase diagram

Next we show the results of magnetic measurements. Fig. 3a shows the temperature dependence of magnetization M for R = Tb and $x = 1.0$ with several values of measuring field H, where the ordinate indicates M/H. At $H = 0.1$ kOe, ZFC magnetization gives a sharp peak at about 52 K. With increasing H, the peak height becomes smaller and the curve changes to plateau-like shape. On the other hand, FC magnetization exhibits an apparent departure from the ZFC one below about 50 K for $H = 0.1$ kOe. The irreversibility temperature T_f, at which FC magnetization departs from the ZFC one, decreases significantly with increasing H. These results are typical spin-glass-like behavior and suggest that a freezing of magnetic moments occurs below these temperatures. Such a spin-glass-like behavior has also been observed in samples with $x \geqslant 0.5$. Similar results were obtained in the series of R = Dy, Er, and also in light series of R = Pr, Nd, and Sm.

Fig. 3b shows the magnetization curves of up to 150 kOe in the R = Tb samples with $x = 1.0$, 0.7 and 0.5 measured at 4.2 K. Large hystereses were observed for all three samples, in which the magnetization changes discontinuously at the coercive field H_c in the samples with $x = 0.7$ and 0.5. The ratio of magnetization at $H = 0$ to that at $H = 150$ kOe is less than 1/2 in the $x = 0$ sample, and increases with decreasing x. It should be noted that for $|H| > |H_c|$ the irreversibility in magnetization is fairly small in samples with $x \leqslant 0.7$ which show apparent discontinuity at H_c.

We have measured the magnetization curves for the R = Tb, Dy, and Er series at various temperatures between 4.2 and 300 K. Obtained values of H_c for R = Tb series are plotted as a function of temperature, as shown in Fig. 4. The H_c values

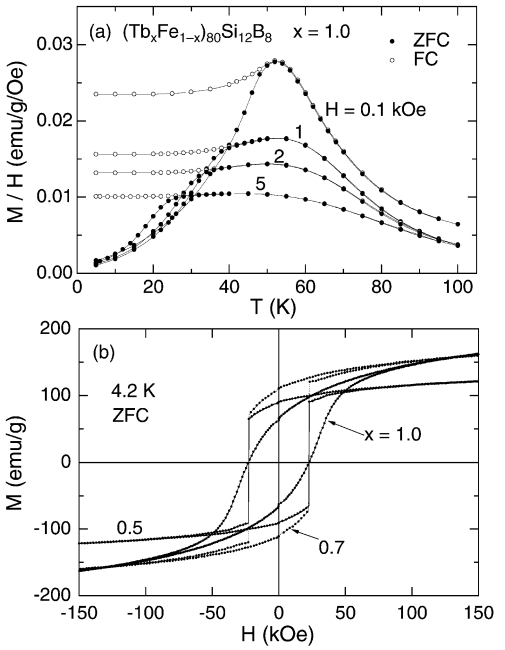

Fig. 3. (a) Temperature dependence of magnetization M in $(Tb_xFe_{1-x})_{80}Si_{12}B_8$ with $x = 1$, with several values of measuring field H, where the ordinate indicates M/H. Field-cooled (FC) and zero-field-cooled (ZFC) data are denoted by solid and open circles, respectively. (b) Magnetization curves in $(Tb_xFe_{1-x})_{80}Si_{12}B_8$ with $x = 0.5$, 0.7 and 1.0.

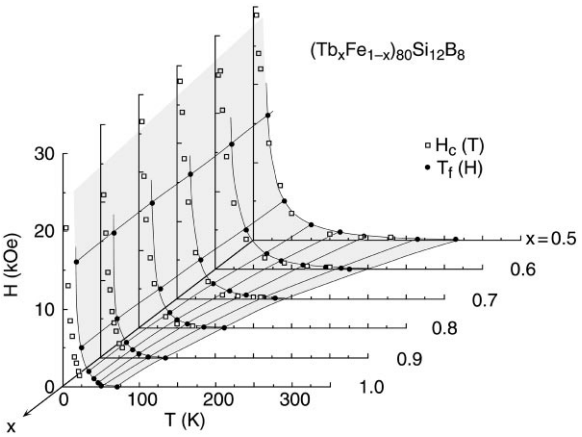

Fig. 4. Field dependence of the freezing temperature $T_f(H)$ obtained from M versus T plots (Fig. 3a), and temperature dependence of the coercive field $H_c(T)$ obtained from M versus H plots (Fig. 3b) for $(Tb_xFe_{1-x})_{80}Si_{12}B_8$ with $x = 0.5$–1.0. Grayed surface is the boundary with which $T_f(H)$ lines are combined together.

shrink drastically with increasing temperature in all the samples. Also shown in these figures are values of the freezing temperature T_f obtained from M versus T measurements at fixed magnetic fields (see Fig. 3a). These figures can thus be regarded as the three-dimensional phase diagrams in H–T–x space. It should be noted that the lines of $H_c(T)$ and $T_f(H)$ are almost identical in the H–T plane especially in samples with $x < 0.7$. Since the irreversibility becomes appreciable both for $T < T_f$ in the M–T curves and for $|H| < |H_c|$ in the M–H curves, the lines of $H_c(T)$ and $T_f(H)$, and hence the grayed surfaces in Fig. 4, are considered to be a good clue to the boundary between the reversible and irreversible regions in the H–T–x space. In the irreversible region of low T and low H side, random freezing of magnetic moments would be realized, where the structure would be speromagnetic for $H = 0$ and sperimagnetic for $H \neq 0$. On the other hand, in the reversible region of high T and high H side, there is neither the field hysteresis nor thermal hysteresis. Near the boundary line in this region, however, there might exist a ferromagnetic correlation between the magnetic moments. The magnetic structure will thus thought to correspond to the FWA state [3,4], where there are some distribution of the directions of magnetic moments around the field direction. Of course, it is difficult to draw a distinct boundary line between FWA and paramagnetic states, since the transition between the two states would be gradual and continuous. In the case of R-rich samples, the difference between the $H_c(T)$ and $T_f(H)$ line becomes appreciable, probably because, in the M–H curves of these samples, the field hysteresis still exist for $|H| < |H_c|$ as shown in Fig. 3b. This fact indicates that H_c is no longer a good index to the irreversibility boundary in these samples. It should be noted that, from Fig. 4, T_f $(H \to 0)$ reduces rapidly with increasing x. This quick decrease would obviously be correlated to the decreasing contribution from exchange interactions between Fe–Fe and Fe–R pairs.

We have made similar measurements for the light R series, in which the coupling between R and Fe magnetic moments is expected to be of

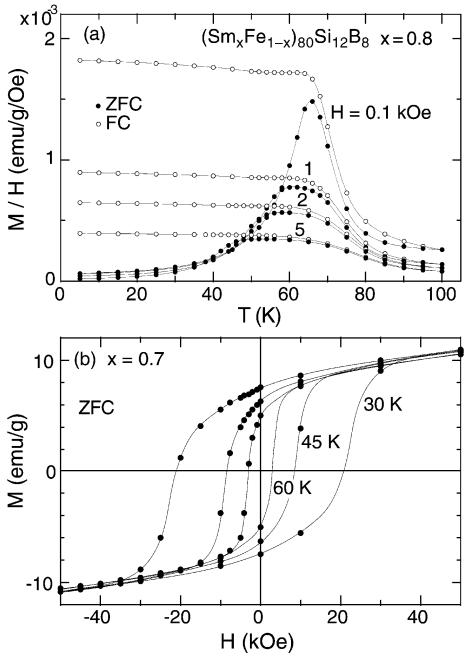

Fig. 5. (a) M/H versus T plots and (b) M versus H plots for $(Sm_xFe_{1-x})_{80}Si_{12}B_8$ with $x = 0.8$ and 0.7.

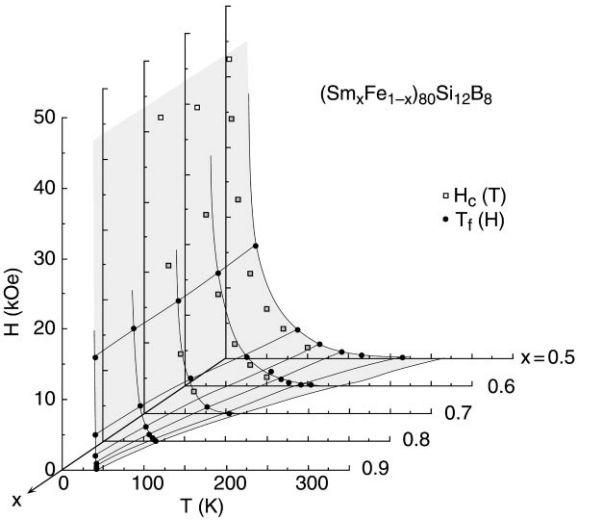

Fig. 6. Same plots as Fig. 4 for $(Sm_xFe_{1-x})_{80}Si_{12}B_8$ with $x = 0.5$–1.0.

ferromagnetic in contrast to the ferrimagnetic one in the heavy R systems. Fig. 5a shows the temperature dependence of magnetization divided by field M/H measured by both ZFC and FC mode for the sample with R = Sm and $x = 0.8$. A sharp cusp is exhibited in the ZFC magnetization for $H =$ 0.1 kOe, while considerable broadening was observed for larger H. Apparent irreversibility between ZFC and FC magnetization values is seen at low temperatures. It should be noted that slight irreversibility is already seen far above the peak temperature of ZFC magnetization. Such high-temperature irreversibility was also observed in samples with R = Dy and Nd.

One example of magnetization isotherms for the $x = 0.7$ sample is shown in Fig. 5b. Since the magnetic anisotropy of Sm-rich samples is so large, external magnetic field of 50 kOe is not enough to align the magnetic moments along the field direction especially at low temperatures. At elevated temperatures, we can anyhow saturate the magnetization and observe hysteresis loops as shown in Fig. 5b. The magnetization in fields of up to 300 kOe has been measured at the first quadrant, which will be presented later in Fig. 7b.

Three-dimensional H–T–x plot for the R = Sm series is displayed in Fig. 6, which is similar to that of R = Tb series given in Fig. 4. It should be noted that, in the R = Sm series, phase boundary line for $x = 0.9$ is almost vertical, which manifests the extreme largeness of RMA.

3.3. High-field magnetization

In order to obtain the direct information about the magnitudes of magnetic moments, we have performed the high-field magnetization experiments in fields of up to 300 kOe at 4.2 K. The results for the R = Tb and Sm series are shown in Fig. 7a and Fig. 7b. The ordinate of these figures are expressed by the averaged magnetic moment value per atom. In the case of R = Tb series, the magnetization values at the highest fields applied are not saturated but continue to increase especially in larger x samples, suggesting that the field is still insufficient to completely align the magnetic moments of R and Fe. It should be noted that not only the magnetization values but also the differential susceptibility increase with increasing x. In the R = Sm series, on the other hand, the magnetization values decrease

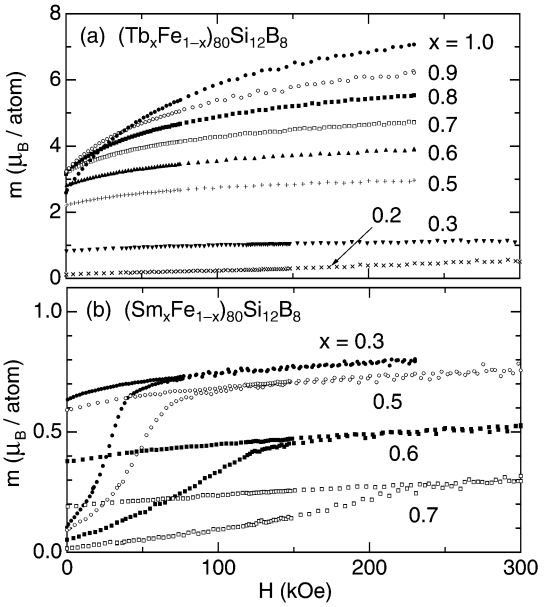

Fig. 7. Magnetization curves in fields of up to 300 kOe for $(R_xFe_{1-x})_{80}Si_{12}B_8$ with (a) R = Tb and (b) Sm, measured at 4.2 K. The ordinate are expressed by the averaged magnetic moment value per atom. Increasing-field data points were omitted in (a) for the sake of clarity.

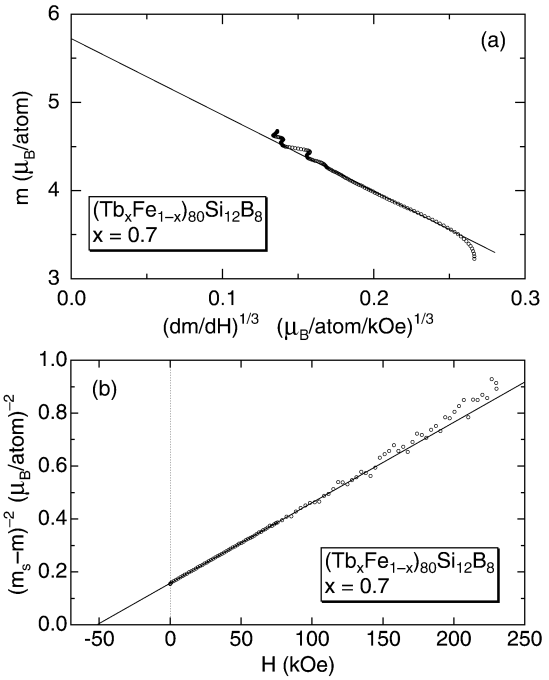

Fig. 8. An example of (a) m versus $(dm/dH)^{1/3}$ plot, and (b) $(m_s - m)^{-2}$ versus H plot for the R = Tb, $x = 0.7$ sample, which determine the saturation magnetization m_s, and the coherent anisotropy field H_{ca}, respectively. Straight lines are the results of least-squares fittings.

with increasing x, which is caused by the small magnitude of Sm magnetic moment m_{Sm}. It is known that m_{Sm} is, in general, as small as 0.2–0.4 μ_B, which is much smaller than $g_J J\mu_B = 0.71$ owing to the hybridization of excited J multiplets [10–12]. The irreversible field H_{irr}, below which magnetization values measured with increasing and decreasing fields are not equal, is very large, reaching about 230 kOe for the $x = 0.7$ sample. It was found that, in samples with $x \geqslant 0.8$, H_{irr} exceeds 300 kOe at 4.2 K. These large values of H_{irr} is caused by the huge RMA of Sm 4f electrons.

In order to obtain a saturation magnetization from the experimental M versus H curves, one in general use a law of approach to saturation [13]. In the case of random anisotropy magnets of small D/J, the ratio of anisotropy to exchange energy, Chudnovsky et al. [3,4] predicted that the deviation from saturation ΔM is proportional to $1/H^{-1/2}$ for $H \ll H_{co}$, and for $H \gg H_{co}$, $\Delta M = 1/H^{-2}$, in which H_{co} is the crossover field. Filippi et al. [14] have analyzed the high-field magnetization curves of amorphous $Dy_xGd_{1-x}Ni$ alloys in the framework of Chudnovsky's theory and determined various parameters including the coherent anisotropy field H_{ca} experimentally. In the present system, however, both R and Fe have magnetic moments and different magnitudes of anisotropy energy, and then, one cannot apply a simple model such as Chudnovsky theory [3,4] or HPZ [15] one. Nevertheless it might be worthwhile to apply the above procedure to the present system and to obtain at least a qualitative information of each series. Fig. 8a is an example of m versus $(dm/dH)^{1/3}$ plot [14] for the R = Tb and $x = 0.7$ sample, giving rise to the saturation magnetization m_s. The coherent anisotropy field H_{ca} has also been evaluated by the plot of $(m_s - m)^{-2}$ versus H as shown in Fig. 8b. In these analyses, the contribution from high-field magnetic susceptibility χ_{HF} has been subtracted by using the data of R = Gd samples, assuming that χ_{HF} only depends on x and does not depend on R. It

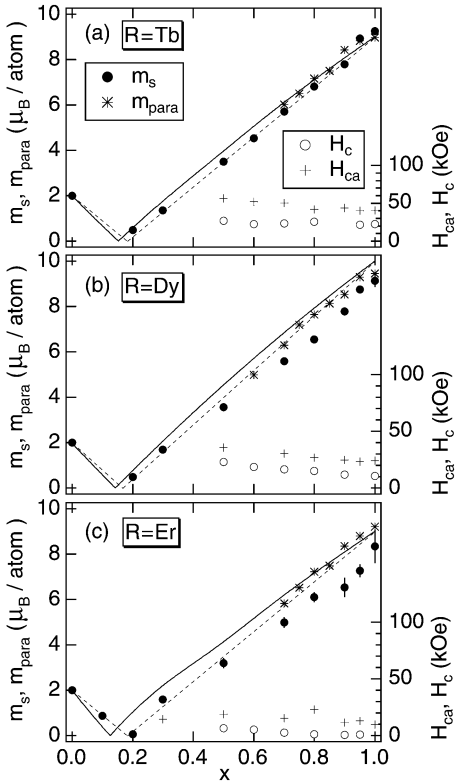

Fig. 9. Saturation magnetization m_s, paramagnetic moment m_{para}, coherent anisotropy field H_{ca}, and coercive field H_c as a function of x for $(R_xFe_{1-x})_{80}Si_{12}B_8$ with (a) R = Tb, (b) Dy, and (c) Er. See text with regard to solid and dashed lines.

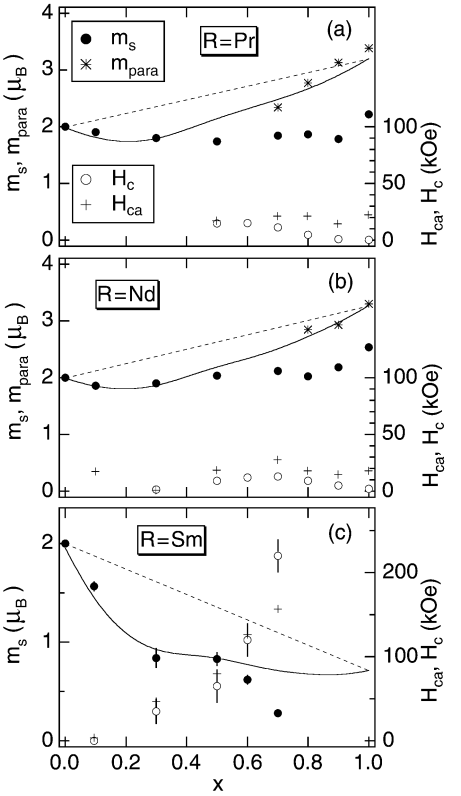

Fig. 10. Same plots as Fig. 9, with (a) R = Pr, (b) Nd, and (c) Sm.

should be noted that the magnitude of the coherent anisotropy field is fairly large ($H_{ca} = 51.7$ kOe) in this sample. This large value of coherent anisotropy will be correlated to the ferromagnetic-like hysteresis curve with large coercive field as shown in Fig. 3b.

By performing the similar analysis given in Fig. 8a and Fig. 8b, we have obtained and plotted in Fig. 9a–Fig. 9c and Fig. 10a–Fig. 10c the values of m_s and H_{ca} as a function of x for heavy R (Tb, Dy and Er) and light R (Pr, Nd, and Sm) series, respectively. In these figures the m_s value of amorphous $Fe_{77}Si_{10}B_{13}$ [9] is plotted as the $x = 0$ value, since it was not possible to produce amorphous $Fe_{80}Si_{12}B_8$. Also shown in these figures are the paramagnetic moment m_{para} obtained from high-temperature susceptibility measurements, and the coercive field H_c at 4.2 K deduced from M–H curves as given in Fig. 3b. The dashed lines in Figs. 9 and 10 indicate the averaged magnetic moment $\langle m \rangle$ per atom defined by

$$\langle m \rangle = |x m_R \pm (1 - x) m_{Fe}|, \quad (1)$$

where we assumed that the R magnetic moment is equal to the full-moment value within the ground J multiplet ($m_R = g_J J \mu_B$) and $m_{Fe} = 2.0\,\mu_B$ irrespective of x. The $\pm$ sign corresponds to the cases of parallel and antiparallel alignments of $\boldsymbol{m}_R$ and $\boldsymbol{m}_{Fe}$, which would in general be realized in light R and heavy R systems, respectively. In the case of R = Tb series, m_s is in good agreement with the lines of $\langle m \rangle$, while for R = Dy and Er series, m_s is appreciably smaller than $\langle m \rangle$ in the R-rich concentration. Solid lines in Figs. 9 and 10, on the other hand, are calculated magnetic moment $\langle m \rangle$ by using Eq. (1), but, now assuming that m_{Fe} is not

constant with 2.0 μ_B but decreases with increasing x, proportional to the averaged hyperfine field $\langle H_{hf}\rangle$, that is, $\langle m_{Fe}\rangle$ given by Fig. 2. The values of paramagnetic moment m_{para} are in better agreement with these solid lines rather than with the dashed lines, suggesting that the total moment is really reduced by the m_{Fe} reduction. In the case of light R series, m_s values are in good agreement with the solid lines for $x < 0.5$, which therefore suggests that m_R is in its full value for $x < 0.5$ and m_{Fe} is reduced as observed by Mössbauer measurements. The discrepancy for $x > 0.5$ will be attributed to the breakdown of the $\Delta M = 1/H^{-1/2}$ formula and also to the reduction of m_R owing to a large CEF potential. In the Sm system, discrepancy for $x > 0.5$ is more serious than those in Pr and Nd series. This will be attributed to the reduction of Sm^{3+} magnetic moment caused by the mixing of excited J multiplets. Another, and more distinguishing situation in Sm^{3+} system is the antiparallel coupling of Sm and Fe moments, which can sometimes be realized by the reversal of spin and orbital contribution of Sm^{3+} owing to the strong hybridization of excited J multiplets. Since the extrapolated moment for $x = 1$ takes negative value as shown in Fig. 10c, such an antiferromagnetic coupling of Sm and Fe moments seems to be realized. Possibility of antiparallel coupling between Sm and Fe moments has been discussed experimentally [16,17] and theoretically [10,18,19].

The magnitude of coherent anisotropy field H_{ca} is the largest in the R = Tb series, and decreases on going from R = Tb to Dy and Er for heavy R systems as shown in Fig. 9. It should be noted that x and R dependence of H_{ca} is correlated to that of the coercive field H_c, although H_c is always smaller than H_{ca}. This correlation seems to be natural, since the coherent anisotropy gives rise to the ferromagnetic remanent magnetization which disappears at the demagnetization field equal to H_c. The magnitude difference between H_c and H_{ca} will be similar to the situation in a normal ferromagnet, in which the observed H_c is always smaller than the anisotropy field H_a, owing to various origins other than the coherent rotation of moments. It should be noted that H_{ca} in Sm series is extremely large especially for $x > 0.5$, which is again correlated to the variation of H_c, although the plotted values of H_c for $x > 0.5$ are not directly measured ones but those estimated from the irreversibility field H_{irr} below which M is irreversible in the first quadrant of M–H curves.

In samples with $x = 1$ which are free from Fe, it is possible to analyze the magnetization process more quantitatively since the only magnetic atom is R. We have made a simple calculation at $T = 0$ K in order to compare the observed magnetization curves for the samples with $x = 1$ with the calculation, and to obtain information about CEF. For simplicity, we neglect the exchange interaction between R atoms, and assume a simplified Hamiltonian for the ith R site:

$$\mathcal{H}_i = A_2^0\langle r^2\rangle\alpha_J O_2^0(i) + A_4^0\langle r^4\rangle\beta_J O_4^0(i) + g_J\mu_B \boldsymbol{J}_i\cdot\boldsymbol{H}, \tag{2}$$

where A_n^0 is the CEF coefficient, $\langle r^n\rangle$ the average of r^n over the radial wave function of the 4f electrons, α_J, β_J the Stevens factors, and O_n^0 the Stevens operator. We assumed here that the z-axis directions of different R sites are randomly distributed and the magnitude of external field $\boldsymbol{H}$ is reduced from a sufficiently large value, i.e., an asperomagnetic arrangement for $H = 0$. The total magnetic moment along the field direction is thus given by

$$m_t = \frac{\sum_i m_i \sin\Theta_i}{\sum_i \sin\Theta_i}, \tag{3}$$

where m_i is the magnetic moment of the ith R along the field direction, Θ_i is the angle between the z-axis of the ith R site and the field direction, with the summation for i running over a hemisphere, i.e., $0 < \Theta_i < 90$. We adjusted the CEF coefficients A_2^0 and A_4^0 so as to best reproduce the observed magnetization curves. The best fit curves together with the observation are given in Fig. 11, and the CEF parameters used in these fits are shown in Table 1. In the case of R = Tb, Dy and Er samples, calculated curves well reproduces the observation for $H > 100$ kOe, while for R = Pr and Nd samples they agree only for $H > 250$ kOe. The reason for the worse fitting in the Pr and Nd samples is the deviation from the axial CEF approximation in RMA system for small J ions, which was discussed by Fert and Campbell [20]. They have shown that the axial CEF is a good approximation to RMA

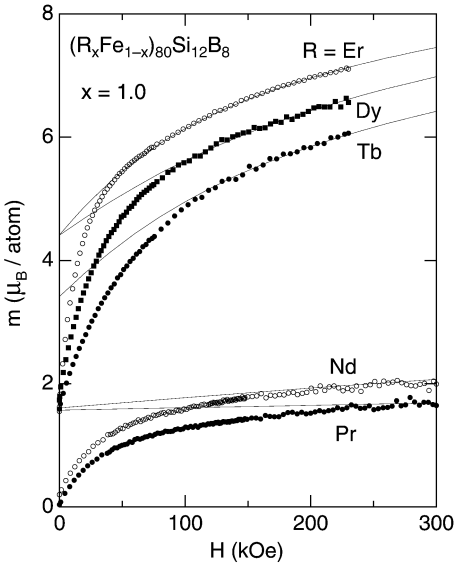

Fig. 11. Calculated total magnetization m_t (solid lines) at 0 K for R = Tb, Dy, Er, Pr, and Nd samples with $x = 1.0$, together with the experiments at 4.2 K. For clarity, origin of the ordinate for R = Tb and Dy are offset by $-1\ \mu_B$ and $-0.5\ \mu_B$, respectively.

Table 1
CEF coefficients for $x = 1$ systems, used in the calculations shown in Fig. 11

R	Pr	Nd	Tb	Dy	Er
$A_2^0(Ka_0^{-2})$	600	400	230	485	−695
$A_4^0(Ka_0^{-4})$	0	0	15	−30	8

system with nonaxial electric field gradients when J is large and that the axial-field model is less justifiable for smaller J and especially non-Kramers ions. A negative A_2^0 for the Er sample as shown in Table 1 is thus consistent to their results [20], since the Stevens factor α_J for Er^{3+} is positive while $\alpha_J < 0$ for Pr^{3+}, Nd^{3+}, Tb^{3+} and Dy^{3+} ions. It should be noted that, for heavy R samples, the fitting has been substantially improved by taking account of the fourth order CEF term, with the magnitudes of A_4^0 being less than 7% of A_2^0, as shown in Table 1.

Fig. 12a shows the magnetization curves for R = Tb, Dy and Er samples with $x = 0.2$. Since $x = 0.2$ is in the vicinity of the compensation composition, magnetization values are very small,

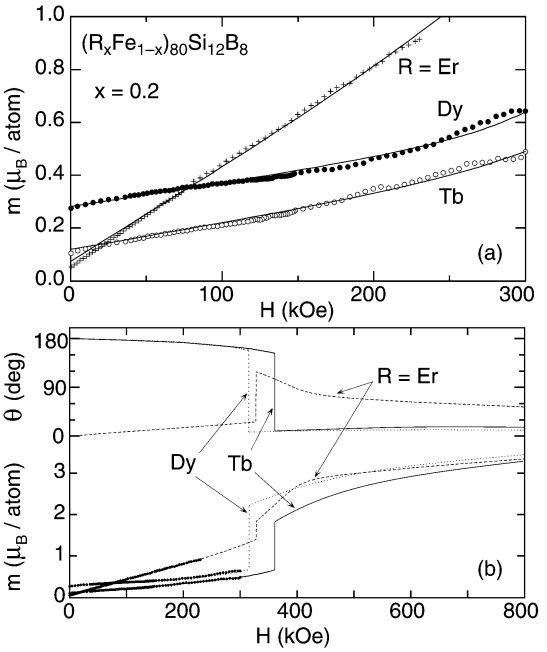

Fig. 12. (a) High-field magnetization curves for R = Tb, Dy and Er samples with $x = 0.2$, measured at 4.2 K. Solid lines are the results of calculations for $T = 0$ using the parameters given in Table 2. (b) The same calculated curves as those in (a) with fields extended up to 800 kOe. Calculated field dependence of Fe moment direction θ is also shown.

showing almost linear field dependence. Moreover, curves for Tb and Dy samples exhibit upward concavity, while the curve for the Er sample shows almost linear field dependence with larger slope. In order to analyze these magnetization curves, we have extended the above formulation to the R_xFe_{1-x} system and calculated the magnetization processes at $T = 0$ K. For simplicity, we assume that all the Fe moments are parallel owing to the strong Fe–Fe exchange interaction, while R moments are asperomagnetic for $H = 0$ as above. We neglect the higher order CEF interactions at the R site. Then the Hamiltonian for the ith R site is written as

$$\mathscr{H}_R^i = A_2^0\langle r^2\rangle\alpha_J O_2^0(i) + 2(g_J - 1)\mu_B \boldsymbol{J}_i \cdot \boldsymbol{H}_m + g_J\mu_B \boldsymbol{J}_i \cdot \boldsymbol{H}, \quad (4)$$

where $\boldsymbol{H}_m$ is the molecular field caused by the Fe–R exchange interaction, which is antiparallel to the Fe

Table 2
CEF and molecular field parameters for $x = 0.2$ samples, used in the calculations shown in Fig. 12

R	Tb	Dy	Er
x	0.33	0.33	0.30
$A_2^0(Ka_0^{-2})$	800	1150	− 550
H_m (K)	25	24	100

magnetic moment $\boldsymbol{m}_{Fe}$. The total energy for the ith R_xFe_{1-x} system is then

$$F_i(\theta) = xE_g^i - (1-x)\boldsymbol{m}_{Fe}(\theta)\cdot\boldsymbol{H}, \tag{5}$$

where E_g^i is the lowest eigenvalue of $\mathscr{H}_R^i$ and θ is the angle between $\boldsymbol{H}$ and $\boldsymbol{m}_{Fe}$. We fixed the magnitude of Fe magnetic moment as $|\boldsymbol{m}_{Fe}| = 2.0\ \mu_B$, and neglect the anisotropy energy of Fe moments. Equilibrium states have been determined so as to minimize the averaged total energy

$$F(\theta) = \frac{\sum_i F_i(\theta)\sin\Theta_i}{\sum_i \sin\Theta_i}, \tag{6}$$

with respect to θ. Calculated results are shown by the solid lines in Fig. 12a, and parameters used are given in Table 2. In this calculation, R concentration x has also been adjusted to be around 0.3 in order to fit the experimental results for $x = 0.2$ samples, since the effective concentration of compensation for $H = 0$ is around $x = 0.3$ owing to the relation $m_R\ (H=0) = \frac{1}{2}g_J J\mu_B$ of the asperomagnetic structure. Fig. 12b shows the same calculated curves with fields extended up to 800 kOe, together with the field dependence of Fe moment direction θ. These results exhibit jumps of magnetization above 300 kOe, owing to the discontinuous rotation of Fe moments. It is thus suggested that observed upward concavity is the incipient stage of metamagnetic-like transition from the speri- to asperomagnetic states. In the case of R = Er, θ $(H = 0)$ is 0°, since the x value used in the calculation (0.30) is smaller than the effective compensation concentration $x_c = 0.31$. Similar fitting with $x > x_c$ has also been examined, which has resulted in an unreasonably large value of H_m.

By comparing Tables 1 and 2, one finds that A_2^0 values for Fe rich samples are much larger than those for Fe free samples in Tb and Dy systems. The reason for the larger A_2^0 in Fe rich sample is not clear at present. One possible explanation will be the difference in the local structure around R ions between Fe rich and Fe free samples. For example, if, in the Fe rich sample, a local arrangement of ligand atoms is more anisotropic, then A_2^0 would be enhanced. It should be noted that A_2^0 values for the Er system are comparable for both concentrations. Again we do not have a conclusive explanation of this result, although there might be different x dependent local structures in the Er system. There will be a correlation between this result and different x dependence of the Fe hyperfine fields shown in Fig. 2 in the Tb, Dy series and other R series including Er.

4. Summary

Now we summarize the present results of $(R_xFe_{1-x})_{80}Si_{12}B_8$ system.

(1) Mössbauer measurements have shown that $\langle m_{Fe}\rangle$ significantly reduces with increasing R content x, being less than 0.5 μ_B for $x = 0.8$ samples.

(2) Low-field magnetization measurements exhibited a typical spin-glass-like behavior for all R series with $x > 0.5$.

(3) Systematic magnetization measurements have revealed that, in H–T space, lines of $T_f(H)$ and $H_c(T)$ coincide well. These lines separate the irreversible and reversible regions.

(4) High-field magnetization measurements and their analysis have shown that the magnitude of saturation moments can be accounted for by assuming m_R being almost equal to the full-moment value $g_J J\mu_B$ for $x < 0.5$. Significant reduction of m_R as compared with the full moment value has been found in the R-rich samples especially for light R series. Antiparallel coupling of Sm and Fe moments has been suggested for the Sm series.

(5) Upward concavity in the high-field magnetization curve has been observed in R = Tb and Dy samples with $x = 0.2$, which was suggested to be an incipient stage of a transition from speri- to asperomagnetic structure, based on the numerical calculations.

Acknowledgements

We are grateful to Messrs. M. Kudo, K. Sai and Y. Ishikawa of High Field Laboratory at IMR for the operation of the hybrid magnets and water-cooled magnets.

References

[1] K. Moorjani, J.M.D. Coey, Magnetic Glasses, Elsevier, Amsterdam, 1984.
[2] R. Ferrer, R. Harris, S.H. Sung, M.J. Zuckermann, J. Phys. C 5 (1979) 221.
[3] E.M. Chudnovsky, W.M. Saslow, R.A. Serota, Phys. Rev. B 33 (1986) 251.
[4] E.M. Chudnovsky, J. Appl. Phys. 64 (1988) 5770.
[5] D.W. Lim, H. Kato, M. Yamada, G. Kido, Y. Nakagawa, Phys. Rev. B 44 (1991) 10014.
[6] J. Hesse, A. Rübartsch, J. Phys. E 7 (1974) 526.
[7] E. Window, J. Phys. E 4 (1971) 401.
[8] S. Ishio, X. Yang, T. Miyazaki, J. Phys.: Condens. Matter 1 (1989) 8979.
[9] S. Ishio, N. Obara, S. Negami, T. Miyazaki, T. Kamimori, H. Tange, M. Goto, J. Magn. Magn. Mater. 119 (1993) 271.
[10] K.H.J. Buschow, A.M. van Diepen, H.W. de Wijn, Phys. Rev. B 8 (1973) 5134.
[11] M. Yamada, H. Kato, H. Yamamoto, Y. Nakagawa, Phys. Rev. B 38 (1988) 620.
[12] H. Kato, M. Yamada, G. Kido, Y. Nakagawa, T. Iriyama, K. Kobayashi, J. Appl. Phys. 73 (1993) 6931.
[13] S. Chikazumi, Physics of Magnetism, Wiley, New York, 1964.
[14] J. Filippi, V.S. Amaral, B. Barbara, Phys. Rev. B 44 (1991) 2842.
[15] R. Harris, M. Plischke, M.J. Zuckermann, Phys. Rev. Lett. 31 (1973) 160.
[16] G. Dublon, M.P. Dariel, U. Atzmony, Phys. Lett. 51A (1975) 262.
[17] H. Adachi, H. Ino, H. Miwa, Phys. Rev. B 56 (1997) 349.
[18] S.K. Malik, S.G. Sankar, V.U.S. Rao, W.E. Wallace, IEEE Trans. Magn. 12 (1976) 1003.
[19] M. Yamada, H. Kato, H. Ido, Y. Nakagawa, J. Magn. Magn. Mater. 140–144 (1995) 867.
[20] A. Fert, I.A. Campbell, J. Phys. F 8 (1978) L57.